



Geotechnical characterization of marine sediments in the Ulleung Basin, East Sea

Changho Lee ^a, Tae Sup Yun ^b, Jong-Sub Lee ^{c,*}, Jang Jun Bahk ^d, J. Carlos Santamarina ^a

^a School of Civil and Environmental Engineering, Georgia Institute of Technology, Atlanta, GA 30332, United States

^b School of Civil and Environmental Engineering, Yonsei University, Seoul, 120-749, Republic of Korea

^c School of Civil, Environmental and Architectural Engineering, Korea University, Seoul, 136-701, Republic of Korea

^d Petroleum and Marine Resources Division, Korea Institute of Geoscience and Mineral Resources, Yuseong, P.O. Box 111, Daejeon, 305-350, Republic of Korea

ARTICLE INFO

Article history:

Received 2 July 2010

Received in revised form 30 September 2010

Accepted 15 October 2010

Available online 27 October 2010

Keywords:

Diatomaceous sediment

Compressibility

Stiffness

Electrical conductivity

Permittivity

Microstructure

Mineralogy

Hydrate-bearing sediments

ABSTRACT

The geotechnical characteristics of Ulleung Basin sediments are explored using depressurized samples obtained at 2100 m water depth and 110 m below the sea floor. Geotechnical index tests, X-ray diffraction, and SEM images were obtained to identify the governing sediment parameters, chemical composition and mineralogy. We use an instrumented multi-sensor oedometer cell to determine the small-strain stiffness, zero-lateral strain compressibility and electromagnetic properties, and a triaxial device to measure shear strength. SEM images show a sediment structure dominated by microfossils, with some clay minerals that include kaolinite, illite, and chlorite. The preponderant presence of microfossils determines the high porosity of these sediments, defines their microstructure, and governs all macroscale properties. The shear wave velocity increases as the vertical effective stress increases; on the other hand, porosity, permittivity, electrical conductivity, and hydraulic conductivity decrease with increasing confinement. All these parameters exhibit a bi-linear response with effective vertical stress due to the crushable nature of microfossils. Well-established empirical correlations used to evaluate engineering parameters do not apply for these diatomaceous sediments which exhibit higher compressibility than anticipated based on correlations with index properties. Settlements will be particularly important if gas production is attempted using depressurization because this approach will cause both hydrate dissociation and increase in effective stress.

© 2010 Elsevier B.V. All rights reserved.

1. Introduction

The Ulleung Basin is a bowl-shaped and back-arc basin bounded by the Korean Peninsula to the west, the Korea Plateau to the north, and the Yamato Ridge and Oki Bank to the east (Fig. 1). The continental shelf of the eastern Korean Peninsula is less than 25 km wide, and it is bordered by a steep slope (4–6°; some local slopes exceed 10°). The opposite side of the basin towards the Yamato Ridge and the Oki Bank consists of a broad shelf (30–150 km) with gentle slope (1–2°). The Ulleung Basin deepens toward the northeast, where it connects to the Japan Basin through the Ulleung Interplain Gap (Lee and Suk, 1998; Bahk et al., 2000). Most sediments in the Ulleung Basin were transported from the continental shelf and slope; in addition, terrigenous materials were contributed by small rivers (Chough et al., 1985; Kwon and Bahk, 2008). They are rich in high plasticity clay minerals and organic matter. These preponderant sandy sediments (i.e., massive sand, bioturbated sand in the shelf) contain laminated and bioturbated clayey layers (Lee et al., 1993; Bahk et al., 2000; Park

et al., 2003, 2007). The gas accumulation in the Late Miocene sand characterizes the petroleum system of the Ulleung Basin. The presence of pockmarks and gas-charged sediments hint at the possible existence of gas hydrate-bearing layers (Huh et al., 1999; Kargl et al., 2006).

The Ulleung Basin Gas Hydrate Expedition 1 (UBGH Expedition 1) took place in the Summer and Fall of 2007 and was organized to explore the presence of gas hydrates (study site in Fig. 1). Seven pressure cores were recovered from 96 m to 136 m below the seafloor at a water depth of ~2100 m. Pressure cores were transferred into storage chambers while maintaining in situ hydrostatic pressure, and kept at ~4 °C and 14 MPa fluid pressure for post-cruise characterization and analyses. Selected cores were depressurized to measure the gas content; then samples were gathered for a comprehensive evaluation of geotechnical properties conducted within 2 months after core extraction. Test devices, procedures, and results are summarized next.

2. Devices—Procedures—Results

Four samples are tested as part of this study. Table 1 summarizes their location, index properties and test methods. Details follow.

* Corresponding author. Tel.: +82 2 3290 3325; fax: +82 2 928 7656.

E-mail address: jongsub@korea.ac.kr (J. S. Lee).

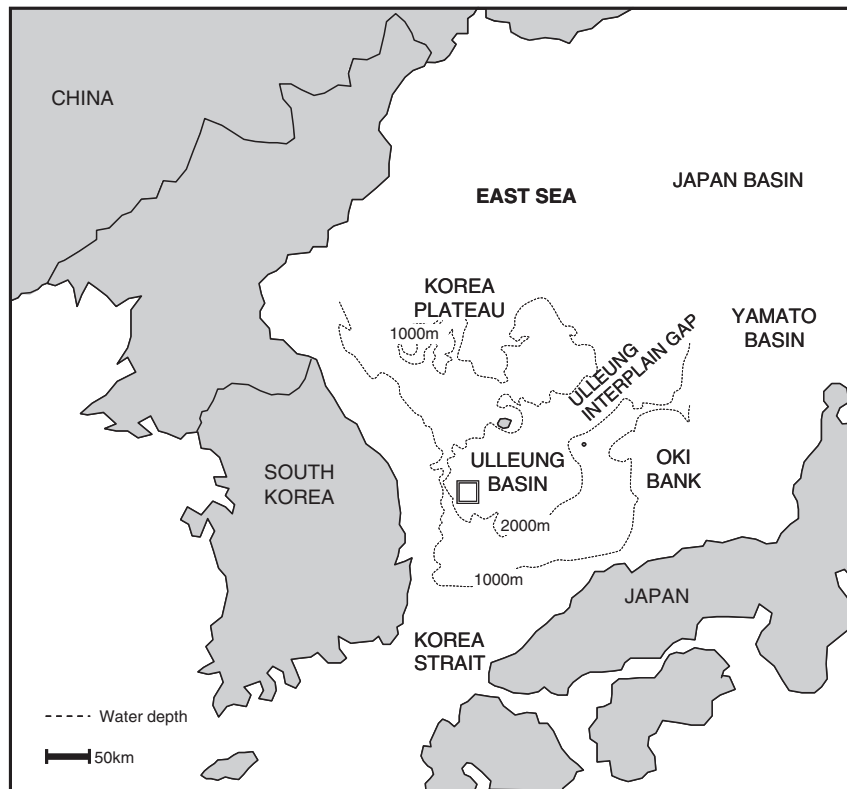


Fig. 1. Location of study site. Cores were recovered from the region shown as a square, within the Ulleung Basin.

2.1. Index properties

Specific gravity: the specific gravity was obtained using a pycnometer (ASTM D854). Measured values range from $G_s = 2.57$ to 2.64 . Previously reported values for this region are in a similar range: $G_s = 2.56$ – 2.61 for sediments in the Ulleung Basin slope (Lee et al., 1993) and $G_s = 2.60$ – 2.66 for Ariake clay (Shiwakoti et al., 2002). Reference values are $G_s = 2.26$ – 2.37 for diatoms and $G_s = 2.65$ for kaolinite.

Grain size distribution: the dynamic scattering method (Microtrac, UPA-150 particle size analyzer) is used to determine the grain size distribution for different specimens. Grain size distribution curves are shown in Fig. 2; for comparison, grain size data are also shown for other hydrate-bearing sediments worldwide. Ulleung Basin sediments are uniformly graded with a median grain size $D_{50} = 2.3$ – $3.0 \mu\text{m}$, similar to previously reported values for this region. Sand seams were found in other cores (Kim and Kim, 2001).

Specific surface: the specific surface area S_a is measured using the N_2 gas adsorption method (Micromeritics Inc., ASAP 2010) and

methylene blue method. Measured values S_a range from 21 to $32 \text{ m}^2/\text{g}$ by gas adsorption and 65 to $110 \text{ m}^2/\text{g}$ by methylene blue. Reference values are $S_a = 10$ – $20 \text{ m}^2/\text{g}$ for diatoms (Locat and Tanaka, 2001) and $S_a = 10$ – $20 \text{ m}^2/\text{g}$ for kaolinite (Mitchell and Soga, 2005). Clay rich hydrate bearing sediments in other regions often exhibit even higher values: 62 to $143 \text{ m}^2/\text{g}$ in the Gulf of Mexico (Yun et al., 2006), 87 to $94 \text{ m}^2/\text{g}$ in the Indian Ocean (Yun et al., 2008); Non hydrate bearing Osaka Bay clayey sediments which contain abundant diatoms, smectite, chlorite, and illite have a specific surface of $S_a = 83$ to $201 \text{ m}^2/\text{g}$ (Tanaka and Locat, 1999).

Atterberg Limits: Atterberg's liquid and plastic limits reflect the effects of specific surface, clay mineralogy, and fluid-dependent soil fabric formation. The measured values of liquid limit $w_L = 67$ – 115% and plastic limit $w_P = 34$ – 65% are plotted on the plasticity chart in Fig. 3. Ulleung Basin sediments fall below the A-line and are classified as either OH, i.e., "organic clay of medium to high plasticity" or MH which agrees with diatomaceous silty clay. For comparison, data for the more plastic Gulf of Mexico, Blake Ridge, and Osaka Bay sediments are superimposed on Fig. 3.

Table 1
Index properties of the Ulleung Basin sediments and measurement methods.

Properties	Sample/Core No.				Method
	9 C-7R	10B-12P	10B-14R	10B-17P	
Core depth [mbsf]	96	118	108	136	
Specific gravity, G_s	2.59	2.61	2.64	2.57	Pycnometer - ASTM D854
D_{50} [μm]	2.279	2.759	2.281	3.041	Dynamic light scattering (UPA-150)
Specific surface, S_a [m^2/g]	20.9	26.7	31.5	30.9	N_2 adsorption
	65.5	73.4	110.7	75.2	Methylene Blue
Passing sieve #200 ($d < 76 \mu\text{m}$)	100	100	100	100	
Liquid limit, w_L [%]	89.7	78.3	66.9	115.0	ASTM D4318-05
Plastic limit, w_P [%]	52.4	40.4	33.8	64.9	
Soil type	OH or MH	OH or MH	OH or MH	OH or MH	Unified Soil Classification System

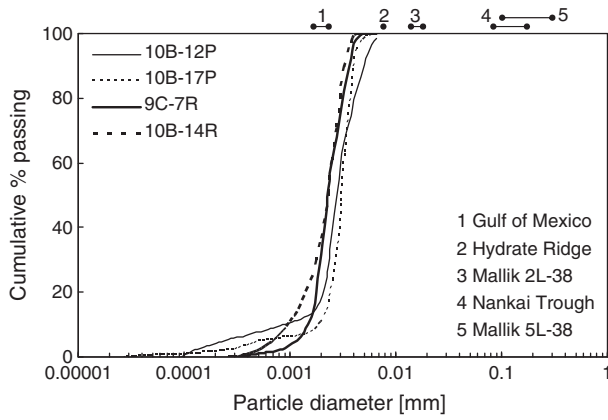


Fig. 2. Grain size distribution—hydrate-bearing sediments from the Ulleung Basin tested in this study. Ranges in mean grain size D_{50} are shown for other hydrate-bearing sediments reported in the literature. References: (1) Francisca et al., 2005; (2) Tan et al., 2006 (3) Jenner et al., 1999 (4) Masui et al., 2006 (5) Jenner et al., 1999.

2.2. Microstructure observation

Scanning electron microscopy was conducted using a Hitachi S-4300 device. Images highlight the abundance of both intact and broken microfossils (both siliceous and calcareous-based on morphology) and some flocculated clay minerals (Fig. 4a–c). Images show dual porosity consisting of inter-grain porosity (μm scale) and intra-grain porosity (submicron). Framboidal pyrite is frequently observed nested in diatoms (Fig. 4c and d). The presence of pyrite suggests dysaerobic conditions during sedimentation (Kim et al., 2003; Rajasekaran, 2006). Pyrite framboids can also form where oxygen is depleted by oxic degradation of benthic infauna. Most pyrite framboids associated with microfossils in the East Sea are thought to have this origin (Bahk et al., 2000). The size of diatoms varies from $10\ \mu\text{m}$ to $150\ \mu\text{m}$, and pyrite framboids are smaller than $\sim 20\ \mu\text{m}$.

2.3. Chemical composition and mineralogy (X-ray diffraction and EDS)

Mineralogy was evaluated using X-ray diffraction (XPERT MPD, Philips, maximum radiation; 3 kW; Fig. 5). Clay minerals are mainly kaolinite with a minor fraction of illite and chlorite. The calcite signature corresponds to microfossils (Tanaka and Locat, 1999).

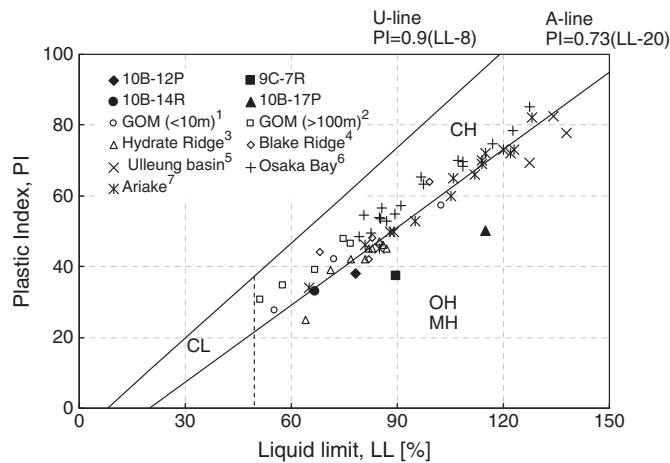


Fig. 3. Liquid and plastic limits shown on the plasticity chart for Ulleung Basin sediments tested in this study and values of the relevant sediments reported in the literature. References: (1) Francisca et al., 2005; (2) Yun et al., 2006; (3) Tan et al., 2006 (4) Winters, 2000 (5) Lee et al., 1993 (6) Tanaka and Locat, 1999; (7) Tanaka et al., 2001.

Previously reported clay minerals include smectite, illite, and kaolinite in the Ulleung Basin (Hillier et al., 1996) and smectite, chlorite, kaolinite, and illite in Ariake clay and Osaka Bay sediments (Tanaka and Locat, 1999; Tanaka et al., 2001). Chemical composition is confirmed using X-ray energy dispersive spectroscopy (Horiba EX-200 with resolution of 138 eV and $10\ \text{mm}^2$). Fig. 5b indicates that the majority of chemical elements are silica (Si), calcium (Ca) and iron (Fe) in agreement with the sediment constitution discussed above. In particular, calcium reflects the abundance of calcareous fossils and shell fragments. A higher content of sulfide (S) and iron (Fe) is observed for framboidal pyrite (Fig. 5c).

2.4. Geomechanical and electrical properties

A zero-lateral strain cell is used to recreate the in situ effective stress conditions (Fig. 6). The cell houses shear wave transducers and a complex permittivity probe. The tested specimens are sliced from cores 10B-17P and 10B-14R, and are kept inside the plastic liner to minimize disturbance. A NaCl solution of equal electrical conductivity as the original pore fluid ($\sigma_f = 3.19\ \text{S/m}$) is added as a supernatant fluid to ensure saturation. The vertical effective stress is incrementally applied to reach a maximum $\sigma'_v = 2.4\ \text{MPa}$ which is more than twice the estimated in situ stress. We monitor volume change, small-strain stiffness (i.e., shear wave velocity), permittivity and electrical conductivity (200 MHz to 1.5 GHz) during both loading and unloading. The first arrivals of the received shear waves are picked up considering the near-field effect (Lee and Santamarina, 2005).

The sediment compressibility is very low up to $\sigma'_v \sim 50\ \text{kPa}$. When the stress exceeds $\sigma'_v \sim 50\ \text{kPa}$, the soil compressibility is characterized by a compression index $C_c = (e_2 - e_1) / \log(\sigma_2 / \sigma_1) = 1.16\text{--}1.19$, as shown in Fig. 7a. Similar compressibility values were reported for sediments obtained at the Ulleung Basin slope in the past ($C_c = 1.11\text{--}1.86$; Lee et al., 1993). During unloading, the swelling index is $C_s = 0.061\text{--}0.075$.

Shear wave velocities measured at each loading stage show a power-type increase with stress for $\sigma'_v > 50\ \text{kPa}$: $V_s = 10.4(\sigma'_m)^{0.4}$ where σ'_m is the mean stress (Fig. 7b). The high value of the exponent $\beta = 0.4$ agrees with the high compression index and reflects changes in interparticle coordination during loading, probably due to microfossil crushing. The shear wave velocity remains high during unloading as the denser fabric remains locked-in, i.e., low C_s (Fig. 7a–b).

Fig. 8 shows the change in hydraulic conductivity during compression estimated from the coefficient of consolidation and the coefficient of volume compressibility based on the 1D consolidation theory (Terzaghi et al., 1996). The value starts at $10^{-5}\ \text{cm/s}$ and rapidly decreases more than 3 orders of magnitude as the void ratio decreases (reference data can be found in Tanaka and Locat, 1999 and Shiwakoti et al., 2002).

The sediment permittivity κ' in the microwave frequency range (upper MHz and GHz) reflects the polarizability of water molecules. Thus, the real permittivity κ' is correlated with the volumetric water fraction of water which is equal to the porosity when the sediment is saturated (Santamarina et al., 2001). Fig. 9a shows the evolution of the permittivity measured in the oedometer cell. The Complex Refractive Index Method-type models superimposed in Fig. 9a are computed with the real permittivity of the mixture. For comparison, lower and upper bounds for the real permittivity can be computed from the mixture components and their volumetric fractions assuming series and parallel configurations (typically wider than the Hashin-Strikman bound): $\kappa'_{\text{mix}} = [n \cdot (\kappa'_p)^c + (1-n) \cdot (\kappa'_f)^c]^{1/c}$, where subscripts mix, p, and fl denote mixture, particles, and fluid. The exponent is $c = -1$ for the series lower bound, and $c = +1$ for the parallel upper bound configuration; the data are well fitted with $c = 0.2$, as shown in Fig. 9 (a).

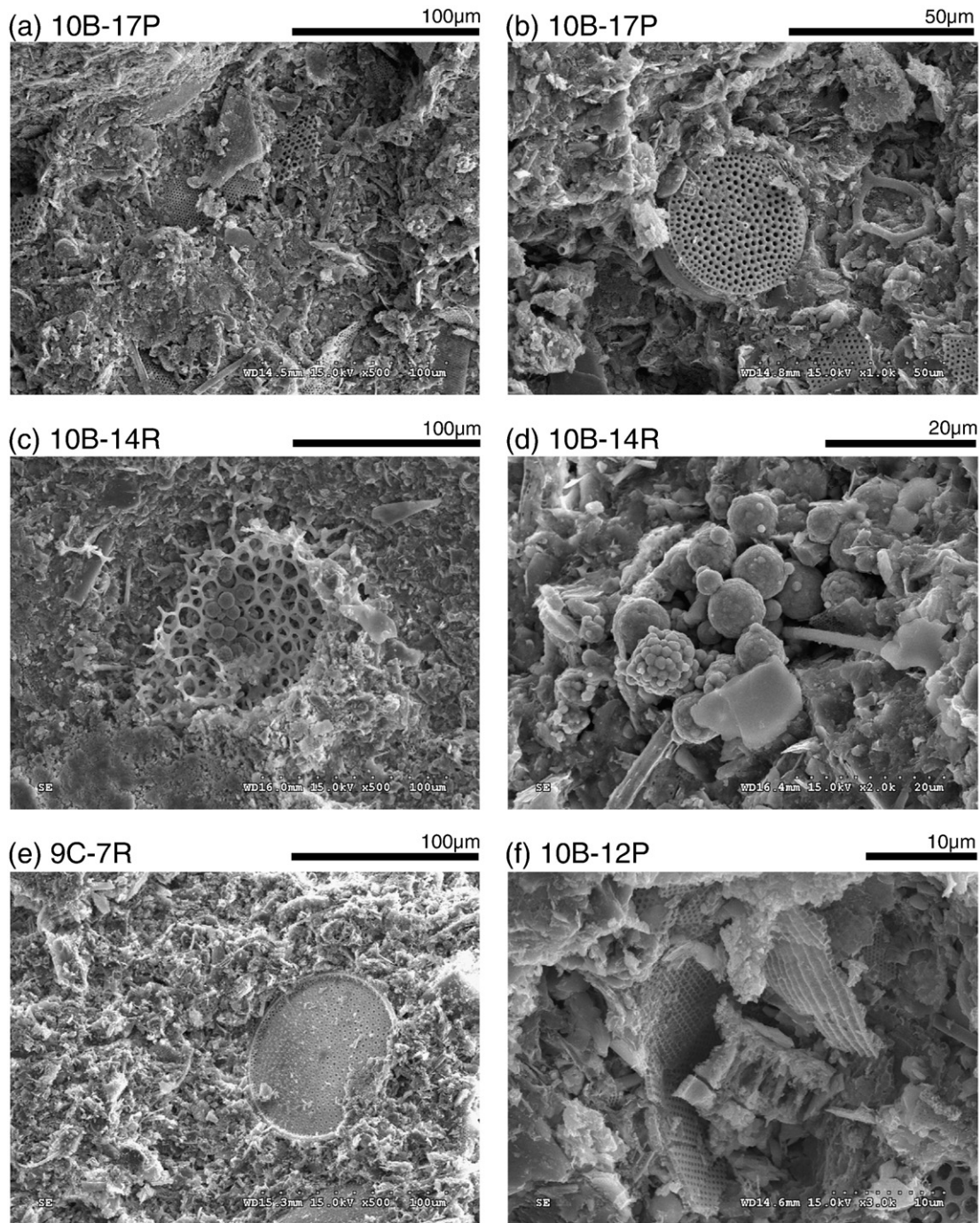


Fig. 4. Scanning electron microscope images. Both intact and broken pieces of diatoms are dominant. Framboidal pyrite is seen in images c and d. Inter (μm) and intra (sub-micron) porosity are readily identified in images b, d, and f.

The sediment electrical conductivity σ_{sed} is determined by the pore fluid conductivity σ_{fl} (i.e., ionic concentration) and volume fraction. Surface conduction is negligible for high-conductivity seawater (Klein and Santamarina, 2005). The simplest form of Archie's law (1942) fits the data well: $\sigma_{\text{sed}} = 1.7 \cdot \sigma_{\text{fl}} \cdot n^{2.8}$.

The sediment shear strength (specimen 10B-17P) is measured using a triaxial device to run undrained axial compression tests with measurement of pore pressure. The three specimens tested are reconstituted by pluviation, and isotropically consolidated to an effective confining stress of 200 kPa. The deviatoric load is imposed in deformation-controlled mode (axial strain rate: 0.5%/h). The measured peak friction angle is $27 \pm 1^\circ$. Previously reported friction angles for Ulleung Basin sediments ranged from 18° to 23° (Lee et al., 1993).

3. Discussions

3.1. Effect of microfossils on physical properties

The preponderant presence of siliceous and calcareous diatoms determines the high volume voids and dual porosity microstructure of these sediments as well as all macroscale properties. Dual porosity explains apparently contradictory properties such as relatively high hydraulic conductivity (determined by large, interconnected inter-particle pores) and relatively high specific surface (determined by the small size intra-particle pores). The fast decrease in hydraulic conductivity with void ratio reported in Fig. 8 reflects the pronounced decrease in large inter-particle pores during loading.

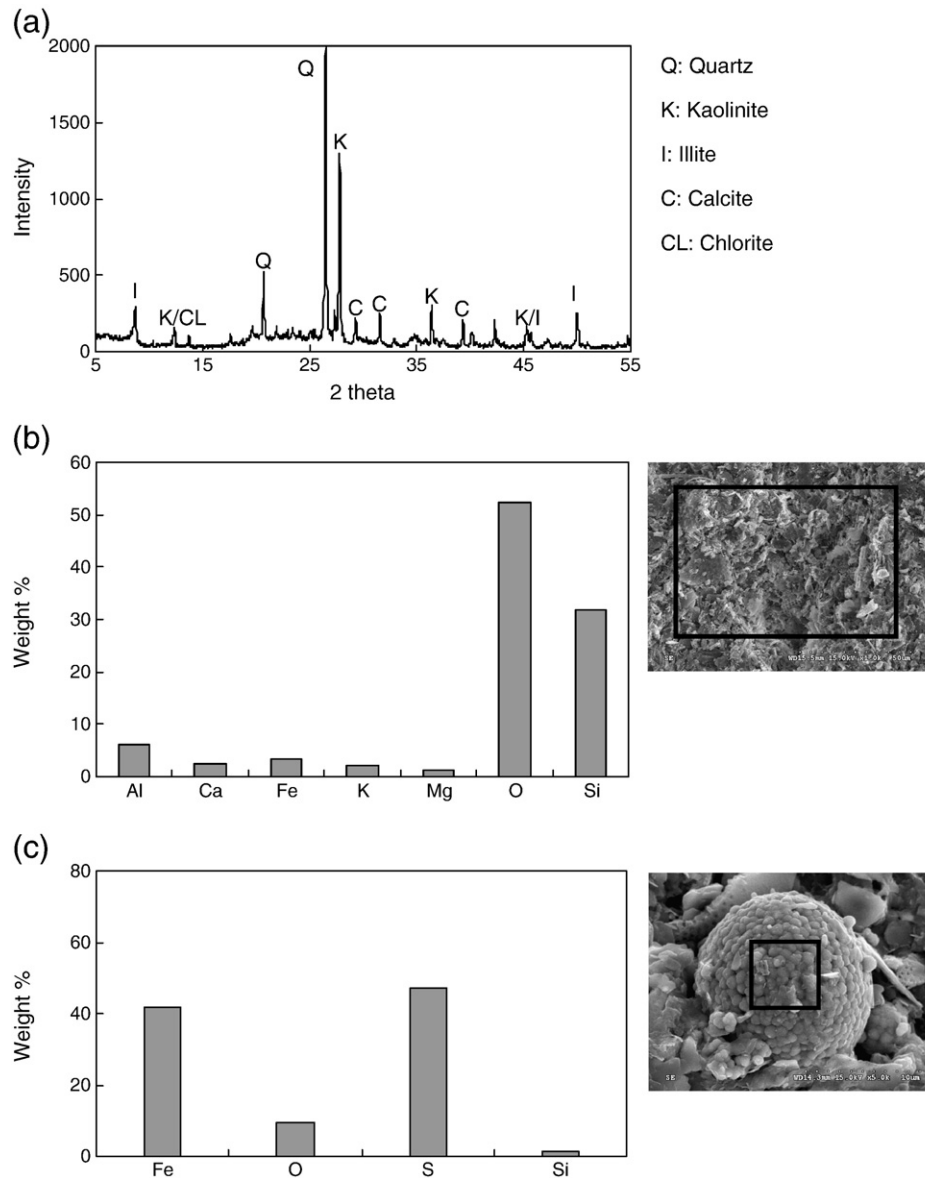


Fig. 5. Mineralogy and composition: (a) Mineralogy of 9C-7R sample measured by X-ray diffraction. (b) Chemical composition of 9C-7R sample measured by X-ray energy dispersive spectroscopy with the corresponding SEM image. (c) Composition of framboidal pyrite of 10B-14R sample.

Diatoms promote interlocking as well as extensive breakage of diatom skeletons during 1D compression and in shear (Shiwakoti et al., 2002; Shigomatsu et al., 2006). In fact, the stability exhibited in e - σ' trends (Fig. 7a) and V_s - σ' results (Fig. 7b) at low effective stress ($\sigma' < 50$ – 80 kPa) corroborates the initially “locked” fabric of diatoms. Thereafter, both grain crushing and particle rearrangement are responsible for the high compressibility (high C_c) and stiffness sensitivity to effective stress (high exponent β in $V_s = \alpha \cdot \sigma'^{\beta}$). The tendency to lock-in fabric also explains the much higher void ratio measured in situ (square symbol in Fig. 7a) than in the same sediment after decompression-reloading. The general definition of $\tan \phi$ in Coulomb’s criterion $\tau = \sigma' \tan \phi$ reflects the “confining stress-dependent shear strength of the soil”. In these diatomaceous sediments, granular breakage is an important energy loss mechanism in shear.

Semi-empirical correlations have been developed in geotechnical engineering to relate index properties to engineering parameters. These correlations are focused on data gathered from natural soils around the world and reflect the most frequently encountered mineralogies. Therefore, their utilization may not be appropriate for diatomaceous marine sediments, such as those

encountered here. For example, consider the following two correlations between compression index C_c and liquid limit LL: $C_c = 0.009(LL-10)$ (Terzaghi et al., 1996), and $C_c = a(LL-b)$ where $0.0046 < a < 0.009$, $8 < b < 12$ (Sridharan and Nagaraj, 2000). Both expressions predict a value for the compression index between $C_c = 0.4$ to 0.9 . However, the compression index for these sediments is between $C_c = 1.16$ (measured here, Fig. 7a) and $C_c = 1.9$ (reported in Lee et al., 1993). As a reference, typical values of compression index for clayey sediments are $C_c = 0.19$ to 0.26 for kaolinite, $C_c = 0.50$ to 1.10 for illite, and $C_c = 1.0$ to 3.6 for montmorillonite (Terzaghi et al., 1996; Sridharan and Nagaraj, 2000; Mitchell and Soga, 2005).

There are pronounced differences in swelling index as well. Correlations in Terzaghi et al. (1996) and in Kulhawy and Mayne (1990) predict a higher rebound capacity ($C_s = 0.09$ to 0.17) than the measured swelling ($C_s = 0.06$ to 0.07). Diatoms may break down during loading and lose their ability to expand upon unloading (Grine and Glendinning, 2007).

The high liquid limit LL and plastic index PI values measured for these diatomaceous sediments and their relatively low specific

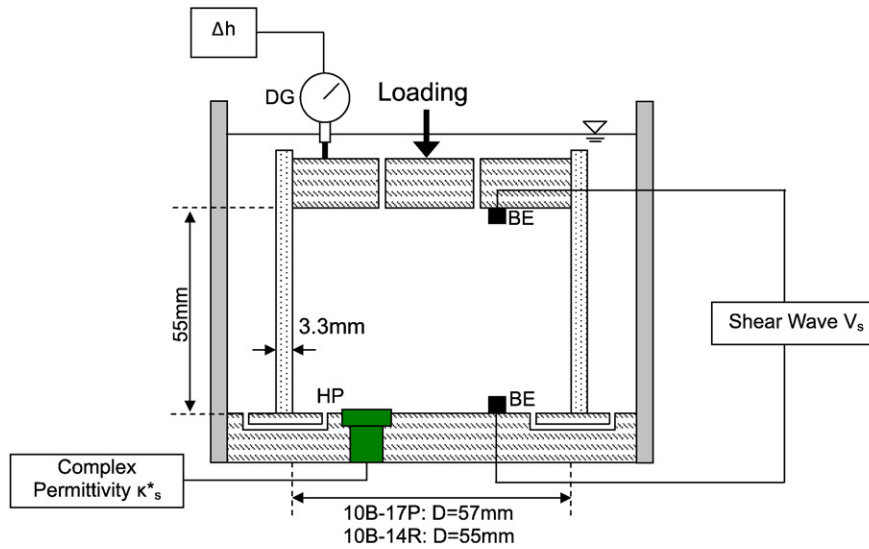


Fig. 6. Instrumented oedometer cell. Transducers include: bender elements BE, dielectric probe HP, and a digital dial gauge DG.

surface area S_a are atypical for soil classification. In fact, the size of diatoms approaches silt-size while the sediment-specific surface resembles that of kaolinite. Thus, differences between this sediment and “standard sediments” call for the in-depth characterization of

these hydrate-bearing diatomaceous sediments and for lower reliance on standard databases.

Diatoms tend to remain intact to effective stress as large as 1 MPa (Tanaka and Locat, 1999; Hong et al., 2006). However, yield stress is lower when specimens are recovered from deep marine diatomaceous sediments due to structural debonding and rearrangement. Furthermore, diatoms in the tested Ulleung Basin sediments exhibit a high degree of chemical and mechanical weathering, forming a weaker and more collapsible structure. In fact, the measured friction angle $\phi = 27 \pm 1^\circ$ is lower than values reported for well-preserved diatomaceous soils $\phi = 33\text{--}40^\circ$ (Shiwakoti et al., 2002).

The in situ void ratio $e_0 = 2.95\text{--}3.15$ is significantly higher than the void ratio measured for the disturbed specimens $e_d = 1.9\text{--}2.1$ at the same vertical effective stress $\sigma'_v = 1.2\text{--}1.4$ MPa (Fig. 7a). The difference is attributed to (1) stable in situ fabric due to diagenetic effects and the presence of hydrate (Hong et al., 2006), (2) evolving into a compressible fabric after disturbance (crushing and extensive particle rearrangement). Therefore, we can anticipate pronounced settlement associated to hydrate dissociation and changes in effective stress (if depressurization ΔP is used for production). A first-order estimate based on measured values follows:

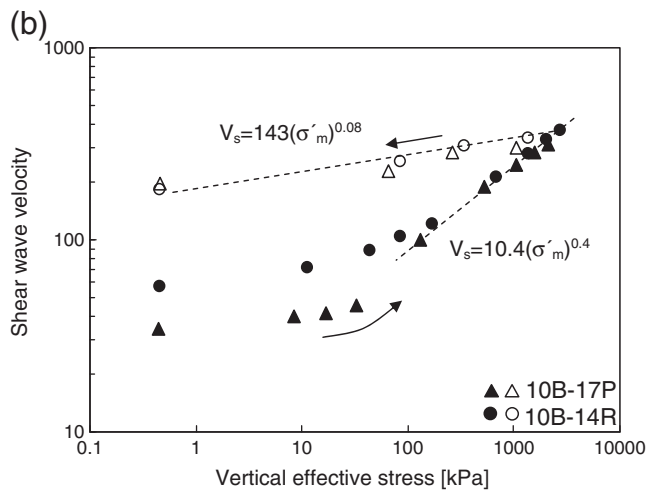
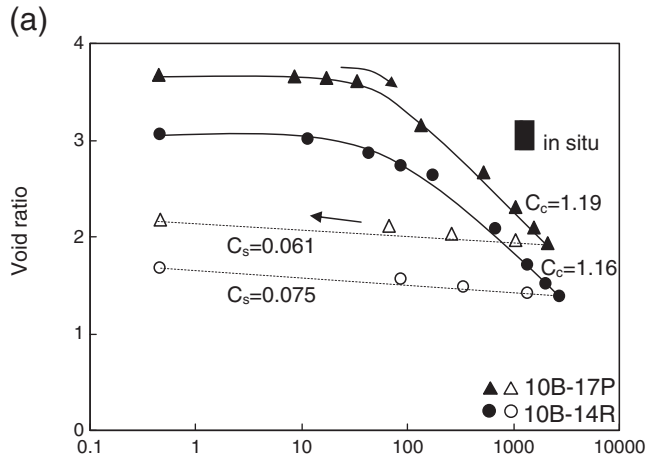


Fig. 7. Evolution of void ratio and shear wave velocity during loading (filled symbols) and unloading (empty symbols). Triangles correspond to specimen 10B-17P and circles to 10B-14R.

$$\varepsilon_{vol} = \frac{e_0 - e_d}{1 - e_0} + \frac{C_c}{1 + e_0} \log\left(\frac{\sigma'_0 + \Delta P}{\sigma'_0}\right) \approx 0.2 + 0.3 \log\left(\frac{\sigma'_0 + \Delta P}{\sigma'_0}\right)$$

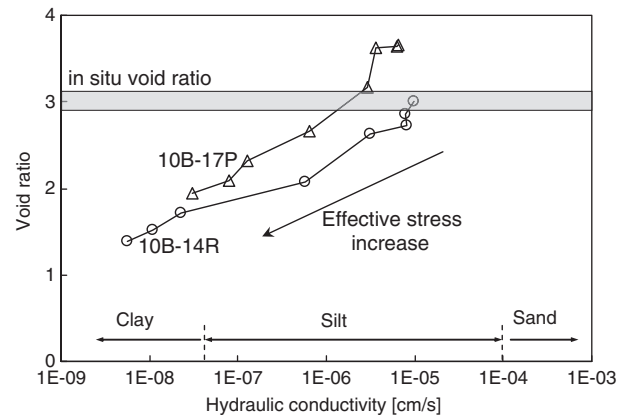


Fig. 8. Estimated hydraulic conductivity vs. void ratio.

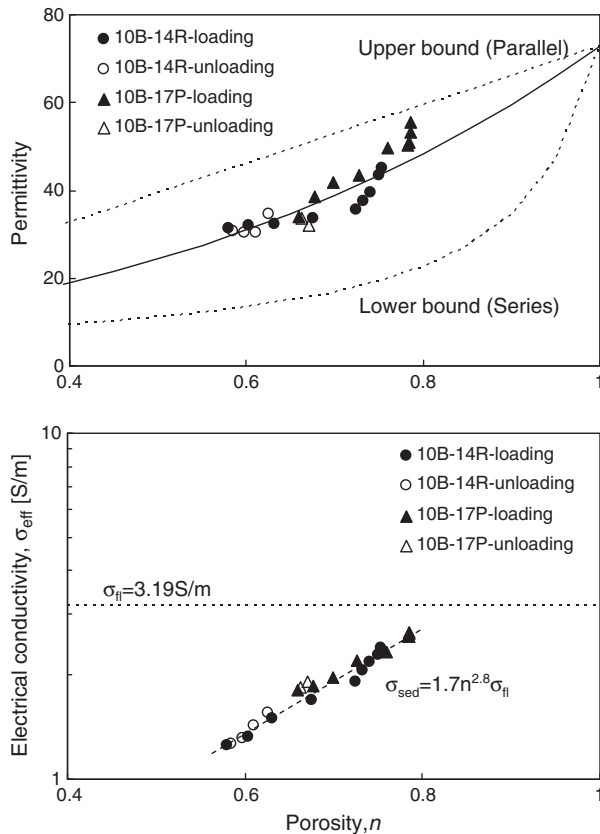


Fig. 9. Permittivity and electrical conductivity (at $f=1$ GHz) vs. porosity.

4. Conclusions

A series of experimental studies are conducted to investigate the characteristics of the deep marine sediments in the Ulleung Basin. The sediments are classified as high-plasticity silts with specific surface $S_a \sim 21$ to $31 \text{ m}^2/\text{g}$. SEM images and XRD data show that sediments consist of microfossils with some illite, kaolinite, and chlorite. Diatoms determine particle size distribution and cause both a dual porosity microstructure, and high initial void ratio. Shear wave velocity increases with the increase in vertical effective stress; the high sensitivity to effective stress is most likely due to particle crushing. Electrical permittivity and conductivity reflect the change in porosity with effective stress. Friction is dominated by the microfossil structure and its breakage. Dual porosity explains the apparent contradiction between high hydraulic conductivity and high specific surface. The closure of the large interparticle pore during loading is responsible for the pronounced decrease in hydraulic conductivity during loading. The microfossil structure biases geotechnical properties and well-established empirical correlations used to estimate engineering parameters may not be applicable. Therefore, differences between “standard sediment response” and these hydrate-bearing diatomaceous sediments call for in-depth experimental characterization and lower reliance on standard databases. The void ratio difference between in situ and disturbed specimens due to (1) diagenetic effects and the presence of hydrate, and (2) evolving into a compressible fabric after disturbance implies that pronounced settlement is anticipated to associate hydrate dissociation and changes in effective stress.

Acknowledgements

This work was supported by the Korea Institute of Geoscience & Mineral Resources (KIGAM), under a research contract to T.S. Yun.

Additional funds to Dr. C. Lee were provided by the Korea Research Foundation Grant funded by the Korean Government (KRF-2008-357-D00271), and to Dr. Santamarina by Chevron Joint Industry Project on Methane Hydrates.

References

- Bahk, J.J., Chough, S.K., Han, S.J., 2000. Origins and paleoceanographic significance of laminated muds from the Ulleung Basin, East Sea (Sea of Japan). *Marine Geology* 162, 19.
- Chough, S.K., Jeong, K.S., Honza, E., 1985. facies of mass-flow deposits in the Ulleung (Tsushima) Basin, East Sea (Sea of Japan). *Marine Geology* 65, 23.
- Francisca, F., Yun, T.S., Ruppel, C., Santamarina, J.C., 2005. Geophysical and geotechnical properties of near-seafloor sediments in the northern Gulf of Mexico gas hydrate province. *Earth and Planetary Science Letters* 237, 16.
- Grine, K., Glendinning, S., 2007. Creation of an artificial carbonate sand. *Geotechnical and Geological Engineering* 25, 441–448.
- Hillier, S., Son, B.K., Velde, B., 1996. Effects of hydrothermal activity on clay mineral diagenesis in Miocene shales and sandstones from the Ulleung (Tsushima) back-arc basin, East Sea (Sea of Japan), Korea. *Clay Minerals* 31, 14.
- Hong, Z., Tateishi, Y., Han, J., 2006. Experimental study of macro- and microbehavior of natural diatomite. *Journal of Geotechnical and Geoenvironmental Engineering* 132 (5), 8.
- Huh, S., Chun, J.H., Han, S.J., Yoo, H.S., Kim, S.R., Kim, H.J., Choi, D.L., Lee, Y.K., 1999. Distribution, characteristics, and depositional environments of gas-charged sediment in the Southeastern Ulleung Basin, the East Sea. *Journal of the Geological Society of Korea* 35 (3), 201–212.
- Jenner, K.A., Dallimore, S.R., Clark, I.D., Paré, D., Mediolli, B.E., 1999. Sedimentology of gas hydrate host strata from the JAPEX/GSC Mallik 2 L-38 gas hydrate research well. In: Dallimore, S.R., Uchida, T., Collett, T.S. (Eds.), *Scientific Results from JAPEX/JNOC/GSC Mallik 2 L-38 Gas Hydrate Research Well, Mackenzie Delta, Northwest Territories, Canada: Geological Survey of Canada, Bulletin*, 544, pp. 57–68.
- Kargl, S., Chenet, P.Y., Yoo, B. and Im, H.G., 2006. Petroleum system analysis for a Back-Arc Basin Offshore South Korea - The Ulleung Basin. Society of Petroleum Engineers, 68th European Association of Geoscientists and Engineers Conference and Exhibition, incorporating SPE EUROPEC 2006, EAGE 2006: Opportunities in Mature Areas. Society of Petroleum Engineers, Richardson, TX 75083-3836, United States, Vienna, Austria, pp. 1819–1824.
- Kim, G.Y., Kim, D.C., 2001. Comparison and correlation of physical properties from the plain and slope sediments in the Ulleung Basin, East Sea (Sea of Japan). *Journal of Asian Earth Sciences* 19, 13.
- Kim, I.S., Park, M.H., Lee, Y., Ryu, B.J., Yu, K.M., 2003. Geological and geochemical studies on the late quaternary sedimentary environment of the southwestern Ulleung Basin, East Sea. *Economic and Environmental Geology* 36 (1), 7.
- Klein, K., Santamarina, J.C., 2005. Behavior of very soft sediments: wave-based monitoring. *International Journal of Geomechanics* 5 (2), 11.
- Kulhawy, F.H., Mayne, P.W., 1990. Manual on estimating soil properties for foundation design, Final Report, Project 1493-6, EL-6800. Electric Power Research Institute, Palo Alto, CA.
- Kwon, Y.K. and Bahk, J.J., 2008. Mass failure and mass flow deposits in the Ulleung Basin and Korea Plateau, East Sea: a Brief Review, Korea Institute of Geoscience and Mineral Resources (KIGAM).
- Lee, J.S., Santamarina, J.C., 2005. Bender elements: performance and signal interpretation. *Journal of Geotechnical and Geoenvironmental Engineering*, ASCE 131 (9), 1063–1070.
- Lee, G.H., Suk, B.C., 1998. Latest Neogene-Quaternary seismic stratigraphy of the Ulleung Basin, East Sea (Sea of Japan). *Marine Geology* 146, 205–224.
- Lee, H.J., Chun, S.S., Yoon, S.H., Kim, S.R., 1993. Slope stability and geotechnical properties of sediment of the southern margin of Ulleung Basin, East Sea (Sea of Japan). *Marine Geology* 110 (1–2), 31.
- Locat, J., Tanaka, H., 2001. A new class of soils: fossiliferous soils? Proceedings of the 15th International Conference on Soil Mechanics & Geotechnical Eng., Istanbul, Turkey, p. 6.
- Masui, A., Haneda, H., Ogata, Y., Aoki, K., 2006. Triaxial compression test on submarine sediment containing methane hydrate in deep sea off the coast off Japan. Proceedings of the 41st Annual Conference, Japanese Geotechnical Society.
- Mitchell, J.K., Soga, K., 2005. Fundamentals of soil behavior. John Wiley and Sons, New Jersey.
- Park, M.H., Kim, I.S., Shin, J.B., 2003. Characteristics of the late Quaternary tephra layers in the East/Japan Sea and their new occurrences in western Ulleung Basin sediments. *Marine Geology* 202, 8.
- Park, M.H., Kim, J.H., Kil, Y.W., 2007. Identification of the late Quaternary tephra layers in the Ulleung Basin of the East Sea using geochemical and statistical methods. *Marine Geology* 244, 13.
- Rajasekaran, G., 2006. Influence of microfossils and pyrites on the behavior of oceanbed sediments. *Ocean Engineering* 33, 13.
- Santamarina, J.C., Klein, K.A., Fam, M.A., 2001. Soils and Waves—Particulate Materials Behavior, Characterization and Process Monitoring. John Wiley and Sons, New York.
- Shigomatsu, H., Higashi, S., Nozowa, M., Yashima, A., 2006. Geotechnical properties of cohesive soil acidified by pyrite inclusion. 5th IEG Environmental Geotechnics: Opportunities, Challenges and Responsibilities for Environmental Geotechnics. Proceedings of the ISSMGE 5th Int. Congress. Thomas Telford

- Services Ltd, London, E14 4JD, United Kingdom, Cardiff, Wales, United Kingdom, pp. 644–650.
- Shiwakoti, D.R., Tanaka, H., Tanaka, M., Locat, J., 2002. Influence of diatom microfossils on engineering properties of soils. *Soils and Foundations* 42 (3), 17.
- Sridharan, A., Nagaraj, H.B., 2000. Compressibility behaviour of remoulded, fine-grained soils and correlation with index properties. *Canadian Geotechnical Journal* 37 (3), 712–722.
- Tan, B., Germaine, J.T., Flemings, P.B., 2006. Data Report: Consolidation and Strength Characteristics of Sediments from ODP Site 1244, Hydrate Ridge, Cascadia Continental Margin. In: Tréhu, A.M., Bohrmann, G., Torres, M.E., Colwell, F.S. (Eds.), *Proceedings of the Ocean Drilling Program*.
- Tanaka, H., Locat, J., 1999. Microstructural investigation of Osaka Bay clay: the impact of microfossils on its mechanical behaviour. *Canadian Geotechnical Journal* 36 (3), 493–508.
- Tanaka, H., Locat, J., Shibuya, S., Soon, T.T., Shiwakoti, D.R., 2001. Characterization of Singapore, Bangkok, and Ariake calcs. *Canadian Geotechnical Journal* 38, 23.
- Terzaghi, K., Peck, R.B., Mesri, G., 1996. *Soil Mechanics in Engineering Practice*, 3rd ed. John Wiley & Sons, New York.
- Winters, W.J., 2000. Stress history and geotechnical properties of sediment from the Cape Fear Diapir, Blake Ridge Diapir, and Blake Ridge. In: Paull, C.K., Matsumoto, R., Wallace, P.J., Dillon, W.P. (Eds.), *Proc. ODP, Sci. Results*, 164, College Station, TX (Ocean Drilling Program), pp. 421–429.
- Yun, T.S., Narsilio, G.A., Santamarina, J.C., 2006. Physical characterization of core samples recovered from Gulf of Mexico. *Marine and Petroleum Geology* 23, 8.
- Yun, T.S., Fatta, D. and Santamarina, J.C., 2008. Hydrate bearing sediments from the Krishna-Godavari Basin: physical characterization of pressure cores and production test Marine geology.